Mathematical Biosciences and Engineering

https://www.aimspress.com/journal/mbe

MBE, 23(3): 619–635.
DOI: 10.3934/mbe.2026024
Received: 22 October 2025
Revised: 16 December 2025
Accepted: 24 December 2025
Published: 27 January 2026

Research article

Spreading of pathological proteins through brain networks: A case study for Alzheimer's disease

Germana Landi[1,*], **Arianna Scaravelli**[1], **Maria Carla Tesi**[1] **and Claudia Testa**[2]

[1] Department of Mathematics, University of Bologna, Italy
[2] Department of Physics and Astronomy "Augusto Righi", University of Bologna, Italy

* **Correspondence:** Email: germana.landi@unibo.it.

Abstract: Given the complexity, unknown causes, and lack of effective treatments for Alzheimer's disease (AD), mathematical modeling offers a valuable approach to its understanding. Models, once validated, offer a powerful tool to test medical hypotheses that are otherwise difficult to directly verify. Here, our focus is to elucidate the spread of misfolded τ protein, a critical hallmark of AD alongside Aβ protein, while taking the synergistic interaction between the two proteins into account. We consider distinct modeling choices, all employing network frameworks for protein evolution, differentiated by their network architecture and diffusion operators. By carefully comparing these models against clinical τ concentration data, gathered through advanced multimodal analysis techniques, we show that certain models replicate better the protein's dynamics. This investigation underscores a crucial insight: when modeling complex pathologies, the precision with which the mathematical framework is chosen is crucial, especially when validation against clinical data is considered decisive.

Keywords: Alzheimer's disease; mathematical models on graphs; $A\beta$ and τ proteins; medical imaging; numerical simulations

1. Introduction

Alzheimer's disease (AD) is an irreversible and incurable neurodegenerative disorder, progressively eroding memory and cognitive function in over 50 million people worldwide, a number projected to surge in the coming years (World Alzheimer Report 2025) [1]. While AD's exact causes remain elusive, two proteins, namely amyloid-beta ($A\beta$) and tau (τ), are central to its emergence and development. Though naturally present in the brain, in AD, they abnormally aggregate into $A\beta$ plaques and neurofibrillary tangles (NFTs), respectively, which are hallmarks of the disease [2–6]. These pathological proteins don't uniformly spread; instead, they follow distinct spatiotemporal patterns [7, 8]. NFTs typically emerge in the entorhinal cortex before spreading throughout the brain, while $A\beta$ plaques initially form

in the temporal and frontal areas [9, 10]. Recent mathematical research highlights the crucial interplay between $A\beta$ and τ, thereby emphasizing its consideration for effective therapies [11–13].

When it comes to modeling the spread of proteins in the brain, a very convenient setting is represented by networks. Indeed, different brain regions are "connected" from a structural point of view by bundles of fibers, and this structure can be very naturally modeled by means of brain networks. A quite commonly used network nowdays is represented by a connectome [14–17]. From a mathematical point of view, a connectome is a weighted graph, in which the vertices represent parcellated regions of gray matter formed by clusters of neurons, which share similarities in cytoarchitecture, functional activity, and structural connections to other regions, while edges represent the connectivity between the regions, which can differ according to the weights. For an updated review on mathematical models, we refer the interested reader to [18, 19], and in particular to [20, 21] for connectome-based models. In [22], we used the Budapest Reference Connectome, v3.0, [23] as a basic connectome: it is a weighted graph that was obtained by averaging the tractography of diffusion tensor images of 477 healthy subjects of the Human Connectome Project [14].

We stress that the vertices of such a graph do not have associated coordinates that determine their position in space, since it is precisely an averaged graph. This will have consequences when we talk about "distances", which must be understood in an intrinsic sense and not in the classical Euclidean metric sense. We use this *structural connectome* to build new connectomes, with the aim of best reproducing some key features of the phenomena we were interested in describing. More precisely, in [22], we introduced two "new" connectomes for the spread of the $A\beta$ and τ proteins. Since the $A\beta$ protein is known to travel on short distances in the extracellular space [24], we constructed what we called the "intrinsic proximity graph", as follows. Given two vertices on the graph, we only connect them if they are close in an intrinsic sense (i.e., only if there already exists an edge connecting them, shorter than a chosen threshold). There is no "vicinity" in an Euclidean metric sense, since the vertices of the graph do not have associated spatial coordinates. Then, we assign weights to the edges that are stronger for intrinsically close vertices. We believe that this modeling choice is reliable, thus also in this work, the $A\beta$ protein will spread along this graph by means of the graph Laplacian operator associated to it.

Unlike $A\beta$, τ is believed to travel over long distances in the intracellular space [25, 26]. To take this feature into account, in [22], we introduced what we called the "cumulative connectome". This connectome is constructed by connecting two vertices of the structural connectome if there is at least one path between them that is shorter than a fixed threshold. The weight of the edge between the two vertices is determined by the sum of the lengths of all paths that connect them. This aggregation of path lengths is what gives the connectome its 'cumulative' nature. In [22], we explored several approaches to model τ spreading and compared the resulting τ concentration values with clinical data. The comparison focused on significant brain regions, where "significant" referred to regions we identified through a statistical analysis of clinical data, thus highlighting differences in τ aggregation between normal and AD brains. Usually, diffusion is modeled either via a Laplacian (in our case a graph Laplacian) or via a convolution operator, especially when long distances are concerned. While for the diffusion of the $A\beta$ protein we simply used the graph Laplacian operator associated to the intrinsic proximity graph, we compared different modeling choices for the spreading of τ. Unsurprisingly, the results in [22] showed that the choice of both the graph on which diffusion takes place and of the mathematical operator used to model it is crucial to achieve a good match with clinical data. The most satisfactory modeling choice turned out

to be the one based on the graph Laplacian associated with the cumulative connectome. This suggests that the cumulative nature of the cumulative connectome is best suited to describe τ diffusion, thereby reflecting, in some sense, the "intrinsic" geometry of the brain. In the wake of this consideration, in this paper, we consider a convolution operator with a kernel built using cumulative paths between brain regions. This choice proves to be decisive to obtain results improved with respect to the ones obtained in [22], where a different choice for the kernel was made. In addition to the introduction of a new kernel, in this paper, we increase the number of significant regions, thereby obtaining satisfactory results.

In summary, the main purpose of this work is to show that both the topology of the graph over which the τ protein spreads and the operator chosen for diffusion are crucial ingredients for a mathematical model that produces a good match with clinical data. The topology of the graph captures the intrinsic geometry of the phenomenon described; therefore, this must be taken into account in the construction of the operator that models the spread, which somehow becomes an operator "intrinsic" to the geometry itself. The paper is organized as follows: in Section 2, we describe the mathematical model, thereby presenting the equations in a quite general form, that is, without explicitly specifying the form of the operators adopted for diffusion or of the graph considered, but carefully explaining all the terms that appear in the equations; in Section 3, we describe the different connectomes (i.e., weighted graphs), and we explicit the form of the different diffusion operators we consider; in Section 4, the procedures adopted to obtain reliable clinical data are explained; in Section 5, we present the results obtained by numerical simulations. By comparisons with clinical data we show the crucial role of the cumulative kernel, and the improvement we obtain here with respect to paper [22]; finally, Section 6 concludes the paper with a discussion and directions for future research.

2. The mathematical model

We are interested in modeling the dynamics of the two proteins, namely $A\beta$ and τ, which are mainly in toxic conformations at least for what concerns τ on a macroscopic scale, that is, when the whole brain is considered. In particular, we would like to understand to what extent the (possibly different) strength of the connections between different brain regions could influence the spread of the proteins in the brain, and more specifically, in brain networks.

The physical concept of brain network finds its ideal mathematical correspondence in the concept of graphs. In this setting, the strength of the connections in the network is represented by the weights associated to the edges of the graph and the structure of the network itself by the connectivity matrix associated with the graph. In AD, τ and $A\beta$ proteins have different biological mechanisms of propagation: $A\beta$ can spread over short distances across brain tissue [24], while τ propagates via a prion-like, neuron-to-neuron mechanism. Moreover, their spreading follows different patterns: τ primarily spreads through neuronal connections, and $A\beta$ initially accumulates in specific cortical regions. Therefore, in our model, we assume that the world in which proteins live, that is, interact and travel, is represented by two different graphs: one for τ and one for $A\beta$. These graphs have the same vertices, which correspond to specific regions of the brain, but different edges, which correspond to different connections between regions. Mathematically, a *graph* is a pair $\mathcal{G} = (V, E)$, where V is a set of vertices and $E \subset V \times V$ is a set of the edges. The graph $\mathcal{G}$ is called weighted if each edge (i, j), which connects vertices i and j, is assigned a weight $w(i, j)$. A weighted graph can be represented through the adjacency matrix A whose entries $A_{i,j}$ represent the weights of the edge (i, j). Let $N = |V|$ be the number of vertices in $\mathcal{G}$; then,

$A \in \mathbb{R}^{N\times N}$ is defined as follows:

$$A_{i,j} = \begin{cases} w(i,j) & \text{if } (i,j) \in E; \\ 0 & \text{otherwise.} \end{cases}$$

There are several possible definitions for the Laplacian associated to a given graph. Given the adjacency matrix $A \in \mathbb{R}^{N\times N}$ of $\mathcal{G}$, following [27], we define the graph Laplacian L as $L = D - A$, where D is the weighted degree matrix whose jth diagonal element $D_{j,j}$ is given by the following:

$$D_{j,j} = \sum_{i=1}^{N} A_{i,j}.$$

In the following, we will denote the Laplacian of the graph for $A\beta$ by $L_{A\beta}$ and the Laplacian of the graph for τ by L_τ.

The full system of equations we are going to study is the one considered in [22], to which we refer for a detailed description, given by the following (all the constants, i.e., greek letters, are positive and $\odot$ denotes the Hadamard product between vectors):

$$\begin{cases} \epsilon \dfrac{d\mathbf{u}_1(t)}{dt} = -\gamma_1 L_{A\beta}\mathbf{u}_1(t) + C_{\mathbf{u}_1} - \alpha\mathbf{u}_1(t) \odot \displaystyle\sum_{j=1}^{3} \mathbf{u}_j(t) - \sigma_1\mathbf{u}_1(t), & \text{(2.1a)} \\ \epsilon \dfrac{d\mathbf{u}_2(t)}{dt} = -\gamma_2 L_{A\beta}\mathbf{u}_2(t) + \dfrac{\alpha}{2}\mathbf{u}_1(t) \odot \mathbf{u}_1(t) - \alpha\mathbf{u}_2(t) \odot \displaystyle\sum_{j=1}^{3} \mathbf{u}_j(t) - \sigma_2\mathbf{u}_2(t), & \text{(2.1b)} \\ \epsilon \dfrac{d\mathbf{u}_3(t)}{dt} = \dfrac{\alpha}{2} \displaystyle\sum_{3\le j+k<6} \mathbf{u}_j(t) \odot \mathbf{u}_k(t) - \sigma_3\mathbf{u}_3(t), & \text{(2.1c)} \\ \dfrac{d\mathbf{w}(t)}{dt} = \gamma_3 K[\mathbf{w}] + C_{\mathbf{w}}(\mathbf{u}_2(t) - U_{\mathbf{w}})^+ + s_{\mathbf{w}}(t) - \sigma_4\mathbf{w}(t). & \text{(2.1d)} \end{cases}$$

The vectors $\mathbf{u}_1, \mathbf{u}_2$, and $\mathbf{u}_3$ represent the molar concentrations of $A\beta$ monomers, dimers, and plaques, respectively, in each node. The ϵ parameter in front of their evolution equations stands for fast dynamics [24]. Monomers and dimers of amyloid-beta do diffuse on short distances in the extra-cellular space, while plaques don't, and this is modeled by the graph Laplacian operator $L_{A\beta}$, which is not present in the equation for plaques. All the terms with σ_i, $i = 1, \dots, 3$ represent clearance, while the remaining terms model aggregation phenomena, and $C_{\mathbf{u}_1}$ is a source term for $A\beta$ monomers. Notice that the factor $\frac{\alpha}{2}$ in Eqs (2.1b) and (2.1c) is there for statistical reasons, to avoid double counting the same term. In the first three equations, relative to the $A\beta$ protein, there is no interaction with τ. The last equation describes the evolution, with slow dynamics, of toxic τ in each node represented by the vector $\mathbf{w}$. The last two terms in the equation model a time dependent source and a clearance (with coefficient σ_4), respectively. As we will see later, the source of toxic τ protein will be localized in the enthorinal cortex [28]. The second term in (2.1d) encapsulates the interaction between the two proteins: a concentration of toxic $A\beta$ above a certain threshold acts as a source for τ. The first term in (2.1d) is crucial in this paper, as it was in [22]. In a possible prion-like mechanism of τ spreading, the misfolded τ protein acts as a template for the healthy one, which in turn misfolds [11]. These phenomena essentially occur in the intracellular space, along axon bundles, and over long distances between non-adjacent brain regions. In order to

understand the temporal pattern of τ spreading, we consider two possible spreading mechanisms on graphs: diffusion and convolution.

When the spreading of τ is modeled via diffusion, by choosing an appropriate graph, we have the following:

$$K[\mathbf{w}] = L_\tau \mathbf{w}, \tag{2.2}$$

where L_τ is the graph Laplacian defined as above via the adjacency and degree matrices of the graph.

When convolution is used to model τ spreading, as is often customary for interactions over long distances, by choosing an appropriate graph, the K operator is defined as follows:

$$K[\mathbf{w}] = U(\hat{\mathbf{k}}_\tau \odot \hat{\mathbf{w}}), \quad \hat{\mathbf{k}}_\tau = U^* \mathbf{k}_\tau, \quad \hat{\mathbf{w}} = U^* \mathbf{w}, \tag{2.3}$$

where $\mathbf{k}_\tau$ is a kernel defined on the graph, U is a matrix whose columns are the eigenvectors of the graph Laplacian L_τ and U^* is the adjoint matrix. We recall that the operator U is used to define the graph Fourier transform [29]; therefore, $\hat{\mathbf{k}}_\tau$ and $\hat{\mathbf{w}}$ are the graph Fourier transform of $\mathbf{k}_\tau$ and $\mathbf{w}$, respectively, and the convolution operator (2.3) is defined as the inverse graph Fourier transform of the element-wise product between $\hat{\mathbf{k}}_\tau$ and $\hat{\mathbf{w}}$. We refer the reader to [22, 30] for a deeper discussion on the graph convolution operator.

The results in [22] showed that the choice of the graph on which the mathematical operators (2.2) and (2.3) are defined is crucial to appropriately reproduce the clinical data. A key contribution of this work consists of having devised a particular graph and defined an appropriate convolution kernel through which we have shown a better matching with clinical data with respect to more standard and commonly used graphs.

3. Proteins spreading through brain's connectomes

As the spreading mechanisms of the τ and $A\beta$ proteins are different, they require distinct structures to be accurately described. Therefore, as already mentioned in Section 2, we use two different graphs: one for Eqs (2.1a)–(2.1c) and one for Eq (2.1d), which are both based on the human "connectome".

The human connectome, which is a map of brain structural networks, is crucial to understand brain diseases. Representing the brain as a graph allows us to assess information processing and transfers. This representation effectively explains two fundamental brain properties: integration and segregation, which balance specialized processing with global coordination. In the graph model, brain regions are vertices connected by edges that represent biological connections. The weights of the edges represent the intensity of the connection between brain regions. The Budapest Reference Connectome, v3.0, [4] is a parameterizable consensus brain graph widely used in the literature. It was derived from the connectomes of 477 people, each computed from MRI datasets of the Human Connectome Project. At the website https://pitgroup.org/connectome/, a high-resolution version with 1015 vertices can be downloaded; the connections between brain regions can be weighted by different factors such as the ratio between the number and the length of fiber tracts that link the vertices or the length of these fiber tracts (the choice of the preferred weight is up to the user). We will refer to this connectome as the *structural connectome* since it was reconstructed using diffusion tensor images.

Mathematically, the structural connectome is a weighted graph $\mathcal{G} = (V, E)$ with $N = 1015$ vertices and weights given by

$$w_{\text{NL}}(i, j) = \frac{n_{ij}}{\ell_{ij}} \tag{3.1}$$

or by

$$w_{\text{L}}(i, j) = \ell_{ij}, \tag{3.2}$$

where n_{ij} is the mean number of fibers connecting vertices i and j, and ℓ_{ij} is the mean length of such fibers, that we will call *fiber length*. We denote the structural connectomes with edge's weights w_{L}, and w_{NL}, by $\mathcal{G}_{\text{L}}$ and $\mathcal{G}_{\text{NL}}$, respectively. Both graphs share the same set of vertices and edges, which correspond to those of the original connectome $\mathcal{G}$; only the weights of the edges differ. We define the convolution operator on the structural connectomes $\mathcal{G}_{\text{NL}}$ and $\mathcal{G}_{\text{L}}$ by using their respective Laplacians to construct the operator U, which defines the graph Fourier transform. We emphasize that, in the following, distances are to be intended in an intrinsic sense (i.e., referring to fiber lengths and not in a geometric sense (i.e., referring to the euclidean distance between two vertices). This choice is the only reasonable one, since we do not know the exact position in space of the vertices of the graph, since the graph is obtained by averaging data from different subjects.

Starting from the structural connectome, in [22], we introduced two new connectomes: the intrinsic proximity connectome and the cumulative connectome. The *intrinsic proximity connectome* is a weighted graph $\mathcal{G}_{\text{P}}$ obtained by connecting two nodes i and j of $\mathcal{G}$ if the fiber length ℓ_{ij} between them is sufficiently small. For such a graph, we fix a threshold R_{P} and define the weights as follows:

$$w_{\text{P}}(i, j) = \begin{cases} e^{-\ell_{ij}^2/\delta_{\text{P}}} & \text{if } \ell_{ij} \le R_{\text{P}} \\ 0 & \text{otherwise} \end{cases},$$

where $\delta_{\text{P}} \in \mathbb{R}^+$ is a fixed parameter. In this way, we only connect two vertices if they are close in an intrinsic sense, instead of a "geometric" proximity measured with some Euclidean distance, and we assign stronger weights to intrinsically closer vertices. Since the $A\beta$ protein is known to spread over short distances in the brain [24], we define Eqs (2.1a)–(2.1c) on the intrinsic proximity connectome and take its Laplacian as operator $L_{A\beta}$.

The *cumulative connectome*, also introduced in [22], is a weighted graph $\mathcal{G}_{\text{c}}$ with the same vertices as $\mathcal{G}$. We recall that, in a weighted graph, the length of a path is obtained as the sum of the weights of all edges along the path. Therefore, in the sequel, we will denote the length of a path p in $\mathcal{G}_{\text{L}}$ and $\mathcal{G}_{\text{NL}}$ as $\ell_{\text{L}}(p)$ and $\ell_{\text{NL}}(p)$, respectively. Given a positive parameter R_{c}, the two vertices i and j are directly connected in $\mathcal{G}_{\text{c}}$ if there is at least one path p in $\mathcal{G}_{\text{L}}$ between i and j whose length $\ell_{\text{L}}(p)$ is at most R_{c}. We call such a path an *admissible path*. The weight $w_{\text{c}}(i, j)$ of the edge between i and j is given by the sum of the lengths ℓ_{NL} of all the admissible paths between i and j:

$$w_{\text{c}}(i, j) = \sum_{p \in \mathcal{A}_{ij}} \ell_{\text{NL}}(p), \quad \mathcal{A}_{ij} = \{p \mid p \text{ is a path in } \mathcal{G}_{\text{L}} \text{ from } i \text{ to } j \text{ and } \ell_{\text{L}}(p) \le R_{\text{c}}\}.$$

We refer the reader to [22] for a deeper description of the cumulative connectome. The cumulative connectome turned out to be the fundamental tool to model, via diffusion, the spreading of the τ protein, which is known to move along long distances in the brain. In fact, an edge between two vertices exists in $\mathcal{G}_{\text{c}}$ if the corresponding brain regions are joined by axonal paths with the length controlled by the parameter R_{c}. The weights of the connections depend on how many and how long the axonal fibers are. For this reason, in this paper, we use the cumulative connectome as the graph to define the operator K when it models the spread via diffusion, and we choose the graph Laplacian of the cumulative connectome for L_τ in (2.2) [22].

The convolution operator (2.3) needs to select a proper kernel $\mathbf{k}_\tau$. In [22], a kernel constructed using the structural connectome with weights w_{L} was considered and gave unsatisfactory results compared to clinical data. In this work, we introduce a new kernel that takes the very nature of the cumulative connectome into account. The cumulative connectome encodes *all* long-range anatomical connections between brain regions, and the strength of these connections depends on the number and length of the axonal fibers. This approach captures the overall strength of the structural connectivity between brain regions. The cumulative nature of this connectome, which integrates all available pathways rather than solely relying on direct connections, represents a novel feature of the model and has shown promising results in aligning model predictions with clinical data [22]. Building on the concept of cumulative connectivity, this work introduces a *cumulative kernel* that incorporates the full spectrum of connections between brain regions. This cumulative kernel, which not only captures direct links but also indirect pathways, provides a richer and more integrative representation of inter-regional interactions. In this way, it offers a powerful tool to model the long-range spread of the τ protein across the brain through graph convolution. Importantly, the convolution is performed in the structural connectomes $\mathcal{G}_{\text{L}}$ and $\mathcal{G}_{\text{NL}}$, using the eigenvectors of their graph Laplacians as the basis for the graph Fourier transform. This formulation allows us to use the spectral properties of the structural connectome to model biologically informed spatial patterns and to encode long-range propagation dynamics of τ protein into the kernel. Let i be a vertex in $\mathcal{G}_{\text{L}}$; we denote the set of vertices that are connected to i through an admissible path by $\mathcal{M}(i)$, i.e.,

$$\mathcal{M}(i) = \{j \in \mathcal{G}_{\text{L}} \,\big|\, \exists \text{ admissible path } p \text{ from } i \text{ to } j\}.$$

First, we define a vector $\mathbf{d} \in \mathbb{R}^N$, where each component d_i quantifies the cumulative connectivity of node i as follows:

$$d_i = \sum_{j \in \mathcal{M}(i)} \sum_{p \in \mathcal{A}_{ij}} \ell_{\text{L}}(p), \quad \mathcal{A}_{ij} = \{p \,\big|\, p \text{ is a path in } \mathcal{G}_{\text{L}} \text{ from } i \text{ to } j \text{ and } \ell_{\text{L}}(p) \le R_{\text{c}}\}.$$

Based on this cumulative measure, we define the cumulative kernel $\mathbf{k}_\tau \in \mathbb{R}^N$ as a node-dependent Gaussian-like weighting function as follows:

$$k_\tau(i) = e^{-d_i^2/\delta_{\text{K}}}, \quad i = 1, \ldots, N, \tag{3.3}$$

where $\delta_{\text{K}} \in \mathbb{R}^+$ is a fixed scaling parameter. Nodes with high cumulative connectivity (large d_i) are assigned higher kernel values, while nodes with lower connectivity are given smaller weights.

4. Materials and methods

We aim to compare the model output with clinical data in brain regions that have undergone significant changes due to AD. We used clinical imaging data to identify such brain regions and to estimate the τ protein concentration values within them. The clinical imaging data for τ were obtained from the ADNI Initiative (ADNI) database (https://adni.loni.usc.edu/). In this paragraph, we briefly recall how the data were obtained, but we refer the reader to [22] for a more detailed description. Our study included 261 participants from ADNI3: 238 cognitively normal (CN) subjects and 23 with AD. All participants were selected based on the availability of both Positron Emission Tomography (PET) scans using the [^{18}F]-AV1451 tracer and the corresponding T1-weighted Magnetic Resonance (MR)

images acquired with a 3T Siemens scanner (MPRAGE sequence), to reduce variability related to scanner type and radiopharmaceutical. PET and Magnetic Resonance Imaging (MRI) acquisitions were required to be within 3 months of each other to minimize the impact of disease progression between the two acquisitions.

The MRI structural images were pre-processed, segmented, and parcellated with FreeSurfer 6.0 (http://surfer.nmr.mgh.harvard.edu/), to subdivide the brain volumes into a set of 83 anatomical cortical and sub-cortical region of interest (ROIs). Since the nodes of the brain graphs are in correspondence with the 83 ROIs, we were able to compare τ concentrations relative to the 83 ROIs in the PET images with those estimated by the mathematical models. To assess differences in [^{18}F]-AV1451 uptake by the brain regions between AD and CN subjects, PET images were co-registered to each subject's corresponding structural MRI using PETSurfer (https://surfer.nmr.mgh.harvard.edu/fswiki/PetSurfer). Then, the τ concentration was computed in each ROI. For absolute quantification, regional τ values were normalized to the cerebellum. Finally, a robust statistical approach, including normality assessment, non-parametric testing, and correction for multiple comparisons, was used to identify ROIs with significantly different τ concentrations between the CN and AD groups. Our statistical analysis revealed that the distribution of ^{18}F-AV1451 uptake was significantly different between the AD and CN groups in 29 ROIs. Table 1 lists the ten most significant ROIs along with their average τ concentrations. Moreover, for each ROI, the table also indicates the corresponding functional network to which it belongs.

Table 1. p-value and τ concentration (mean ± st.dev.) in the AD and CN groups for the most significant ten ROIs. The concentrations of τ are expressed as normalized ratios relative to the concentration measured in the cerebellum.

ROI	Network	Significance	AD τ conc.	CN τ conc.
Fusiform region	Occipital	$8.3 \cdot 10^{-9}$	1.6 ± 0.3	1.2 ± 0.1
Inferior temporal region	Temporal	$1.6 \cdot 10^{-8}$	1.7 ± 0.5	1.2 ± 0.2
Middle temporal region	Temporal	$2.9 \cdot 10^{-6}$	1.6 ± 0.5	1.2 ± 0.2
Lingual region	Occipital	$3.1 \cdot 10^{-6}$	1.4 ± 0.3	1.1 ± 0.1
Lateral orbitofrontal region	Limbic	$5.4 \cdot 10^{-6}$	1.5 ± 0.4	1.2 ± 0.2
Amygdala	Limbic	$6.5 \cdot 10^{-6}$	1.4 ± 0.4	1.2 ± 0.1
Temporalpole region	Temporal	$1.3 \cdot 10^{-5}$	1.4 ± 0.3	1.1 ± 0.2
Enthorinal region	Limbic	$2.1 \cdot 10^{-5}$	1.4 ± 0.4	1.1 ± 0.2
Parsorbitalis region	Frontal	$2.6 \cdot 10^{-5}$	1.5 ± 0.5	1.2 ± 0.3
Lateraloccipital region	Occipital	$2.7 \cdot 10^{-5}$	1.5 ± 0.6	1.2 ± 0.2

5. Results

A series of numerical simulations was performed to determine whether the diffusion-based or convolution-based formulation of the operator K provides a better representation of the clinical imaging data. All simulations were conducted using Matlab R2021a on an Intel Core i5 processor with 2.50 GHZ and a Windows operating system. The codes used for the current experiments can be made available upon reasonable request to the authors.

5.1. Experimental setting

We used the same experimental setting described in [22]. The differential system (2.1) was numerically solved using Matlab's `ode45`, which implements the Dormand–Prince Runge–Kutta method with adaptive time stepping [31]. The system was integrated from the initial time $t_0 = 0$ to the final time $t_f = 500$, which was chosen to ensure the stabilization of the solutions. The source term for misfolded τ was set in the enthorinal region, which is the brain region that exhibits the earliest τ deposits in AD; i.e.,

$$(s_{\mathbf{w}}(t))_j = \begin{cases} 1 & j \in \text{ entorhinal region} \\ 0 & \text{otherwise} \end{cases}, \tag{5.1}$$

where $(s_{\mathbf{w}}(t))_j$ denotes the jth component of $s_{\mathbf{w}}(t)$. We assume that the clinical data used to fit the numerical output correspond to a stage in which the disease is well established. Consequently, we interpret this state as an asymptotic equilibrium point reached in the infinite time limit. From a mathematical perspective, this implies that the protein concentrations no longer evolve over time but remain constant. In the numerical simulations, when the output stabilizes at a constant value, we consider the equilibrium point to have been reached. Naturally, the specific constant value depends on the chosen parameter set; therefore, we regard those parameters that yield numerical solutions whose limit values are consistent with the clinical data as optimal. These optimal values were heuristically identified by performing extensive trials over wide grids of possible values. This approach allowed us to identify values that yielded a stable equilibrium point for the dynamical system, thus ensuring biologically plausible and mathematically consistent behaviors. According to the above strategy, in our numerical simulations, we fixed the values of all parameters of system (2.1) as reported in Table 2, except γ_3 and $C_{\mathbf{w}}$.

Table 2. Fixed parameter values for system (2.1).

γ_1	γ_2	α	$C_{\mathbf{u}_1}$	$U_{\mathbf{w}}$	σ_1	σ_2	σ_3	σ_4
0.001	0.001	0.1	0.05	0.01	0.1	0.1	0.1	0.11

As described in Section 3, we modeled the spreading of the $A\beta$ protein on the intrinsic proximity connectome $\mathcal{G}_{\text{P}}$, where the values $R_{\text{P}} = 25$ and $\delta_{\text{P}} = 1.5 \cdot 10^2$ were fixed. When the spreading of the τ protein was modeled through a diffusion operator, the underlying network structure was represented by the cumulative connectome $\mathcal{G}_{\text{c}}$ with $R_{\text{c}} = 30$. Finally, when employing a convolution operator to model the spreading of τ protein, we used the structural connectome $\mathcal{G}$ and compared the two different weighting schemes: one based on fiber lengths, and the other on the ratio between the number of fibers and their lengths. This led us to define two distinct Fourier transform operators: U_{NL}, which corresponds to the structural graph with weights w_{NL}; and U_{L}, which corresponds to the graph with weights w_{L}. These operators encode different spectral properties of the connectome and are used to analyze the τ protein dynamics under convolution. In both cases, the kernel $\mathbf{k}_\tau$ is defined by (3.3) with $\delta_{\text{K}} = 10^{-4}$.

5.2. Clinical deterioration pattern and model evaluation

In this work, we adopted the same methodology used in our previous paper [22] to evaluate the agreement between model predictions and clinical data. This approach is based on comparing the

clinical deterioration pattern, which is derived from τ concentrations in significative brain regions (as identified in Section 4), with the pattern predicted by the mathematical model. While in our previous study we only considered six ROIs, selected according to a statistical threshold with p-values up to the order of 10^{-6}, in the present work we extended the analysis to ten ROIs, thereby including regions with p-values up to the order of 10^{-5}. The ten ROIs considered are listed in Table 1, along with the functional networks to which they belong. Moreover, to assess the models' ability to distinguish affected from unaffected regions, we also considered the τ concentration in the sensorimotor network, including the paracentral, postcentral, precentral, and superior frontal regions, which is typically unaffected in AD pathology.

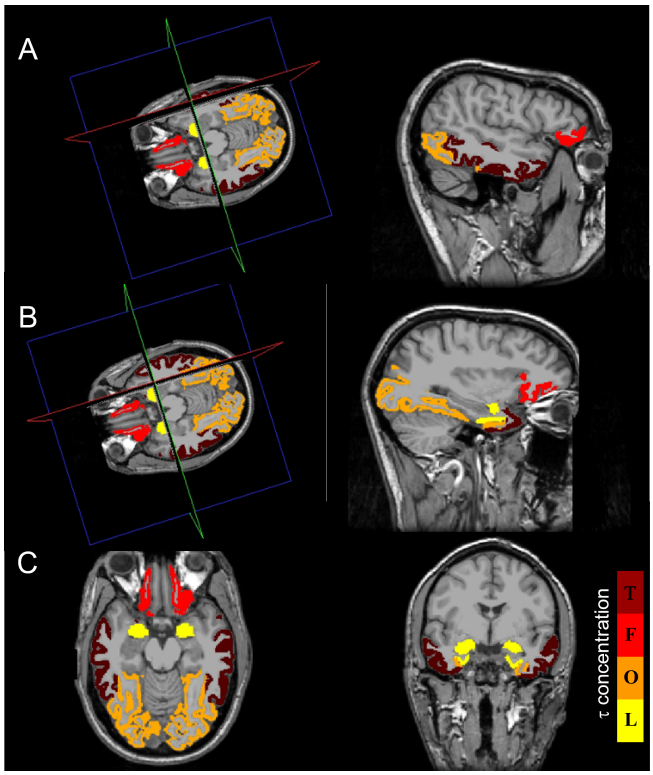

Figure 1. Mean τ concentration values $w_T^{(*)}$, $w_O^{(*)}$, $w_L^{(*)}$, $w_F^{(*)}$ in the temporal, occipital, limbic and frontal networks as listed in Table 1. The colorbar reflects the ordering of τ values, from high (dark red) to low (yellow). A: 3D view of the brain and the corresponding sagittal plane. B: 3D view of the brain and the corresponding sagittal plane. C: corresponding axial and coronal view.

We denote the mean τ values averaged over the significant ROIs that belong respectively to the temporal, occipital, limbic and frontal networks by $w_T^{(*)}$, $w_O^{(*)}$, $w_L^{(*)}$, $w_F^{(*)}$, respectively, as detailed in Table 1. Each $w_X^{(*)}$ represents the mean τ value across all significant ROIs within the corresponding network X. Figure 1 represents the mean τ concentration values $w_T^{(*)}$, $w_O^{(*)}$, $w_L^{(*)}$, $w_F^{(*)}$ in the four networks.

In addition, we denote the mean τ value in the sensorimotor netwok by $w_S^{(*)}$. The values $w_T^{(*)}$, $w_O^{(*)}$, $w_L^{(*)}$, $w_F^{(*)}$, $w_S^{(*)}$ form a reference profile derived from clinical data and ordered from highest to lowest τ concentration, which yield a string that we define as the *clinical deterioration pattern*. This pattern reflects the spatial progression of neurodegeneration in AD, with higher τ levels indicating

more severe deterioration. In [22], we considered six ROIs (grouped into three networks) and we obtained the clinical deterioration pattern represented by the string TLOS since $w_T^{(*)} > w_L^{(*)} > w_O^{(*)} > w_S^{(*)}$. In this work, with ten ROIs (grouped into four networks), the corresponding string becomes TFOLS. We notice that when ten ROIs are considered, not only does a new network (the Frontal one) occur, but additional regions also contribute to the values $w_T^{(*)}, w_O^{(*)}, w_L^{(*)}, w_S^{(*)}$.

To evaluate the ability of the mathematical model (2.1) to reproduce the clinical deterioration pattern, we numerically solve the differential system and compute the average τ concentrations over the same brain networks considered in the clinical analysis. This is possible since we precisely know to which region each vertex belong to in the graph (the connectome). Then, these values are used to construct a string based on the descending order of τ concentrations.

Then, we compare the model's deterioration pattern to the clinical reference one using the *Hamming distance (HD)*, which counts the number of mismatches between the two strings. A lower HD indicates a closer match to the clinical progression of the disease. This approach provides a quantitative framework to assess how well the mathematical model captures the spatial dynamics of τ pathology in AD, both in affected and preserved brain regions.

5.3. Numerical results

Here, we present the numerical results obtained by solving the differential system (2.1) for the following choices of the operator K: diffusion on the cumulative connectome $\mathcal{G}_{\text{C}}$ and convolution on the structural connectomes $\mathcal{G}_{\text{L}}$ and $\mathcal{G}_{\text{NL}}$. Tables 3 and 4 show the string that corresponds to the minimal HDs obtained for each configuration, together with the parameter values that allow the model to reproduce it. Table 3 refers to the case with six ROIs and the deterioration string TLOS, while Table 4 refers to the case with ten ROIs and the string TFOLS. The parameters $C_{\mathbf{w}}$ and γ_3 were heuristically identified in each case to minimize the HD between the clinical and simulated deterioration patterns. For each parameter, we observed intervals of values that yield the same minimal HD; in the tables, we report one representative value per parameter.

Table 3. Deterioration patterns and model parameters for different choices of the operator K, using six ROIs.

Operator K	String	HD	γ_3	C_w
Clinical data	TLOS	–	–	–
Diffusion on $\mathcal{G}_{\text{C}}$	TLOS	0	0.002	1.58
Convolution on $\mathcal{G}_{\text{L}}$	TSOL	2	0.002	1.58
Convolution on $\mathcal{G}_{\text{NL}}$	TLOS	0	0.002	1.58

From Tables 3 and 4, we observe that the diffusion operator on the cumulative connectome $\mathcal{G}_{\text{C}}$ is only able to reproduce the deterioration pattern TLOS, which corresponds to the configuration with six ROIs. Similarly, the convolution operator on the structural connectome $\mathcal{G}_{\text{NL}}$, where edge weights are defined as the ratio between the number of fibers and their length, also only reproduces the TLOS pattern. On the other hand, the convolution operator on the length-based graph $\mathcal{G}_{\text{L}}$ is the only one capable of reproducing the deterioration pattern TFOLS, which is associated with the configuration that involves ten ROIs. Comparing the results obtained with 6 ROIs with those obtained with 10 ROIs, a sort of "complementarity" stands out: what works best in one case works worse in the other. This

shows that selecting the graph is an integral part of the modeling process and should be carried out with great attention.

Table 4. Deterioration patterns and model parameters for different choices of the operator K, using ten ROIs.

Operator K	String	HD	γ_3	C_w
Clinical data	TFOLS	–	–	–
Diffusion on $\mathcal{G}_{\text{C}}$	FTOLS	2	0.001	50
Convolution on $\mathcal{G}_{\text{L}}$	TFOLS	0	0.009	50
Convolution on $\mathcal{G}_{\text{NL}}$	FTOSL	4	0.002	1.58

Table 5. Deterioration patterns and model parameters for different choices of the operator K, using six ROIs.

Operator K	String	HD	γ_3	C_w
Clinical data	TLOS	–	–	–
Diffusion on $\mathcal{G}_{\text{L}}$	LTOS	2	0.001	0.5
Diffusion on $\mathcal{G}_{\text{NL}}$	LTOS	2	0.001	0.5
Convolution on $\mathcal{G}_{\text{L}}$	TOSL	3	50	0.5
Convolution on $\mathcal{G}_{\text{NL}}$	LSTO	4	150	0.5

Table 6. Deterioration patterns and model parameters for different choices of the operator K, using ten ROIs.

Operator K	String	HD	γ_3	C_w
Clinical data	TFOLS	–	–	–
Diffusion on $\mathcal{G}_{\text{L}}$	FTOSL	4	0.001	0.5
Diffusion on $\mathcal{G}_{\text{NL}}$	FTOLS	2	0.001	0.5
Convolution on $\mathcal{G}_{\text{L}}$	FOLTS	4	50	0.5
Convolution on $\mathcal{G}_{\text{NL}}$	FSTLO	4	150	0.5

To further highlight the importance of incorporating cumulative connectivity, we consider two alternative approaches: diffusion on the structural connectomes $\mathcal{G}_{\text{NL}}$ and $\mathcal{G}_{\text{L}}$, and convolution on $\mathcal{G}_{\text{NL}}$ and $\mathcal{G}_{\text{L}}$ with a kernel that does not exploit cumulative information. In the latter case, the kernel $\mathbf{k}_\tau^{\text{sp}} \in \mathbb{R}^N$ is constructed using the shortest-path distances from each node to all others, which is defined as follows:

$$k_\tau^{\text{SP}}(i) = \sum_{j \in \mathcal{G}_{\text{L}}} e^{\ell_{ij}^{\text{SP}}/\tilde{\delta}_{\text{K}}}, \quad i = 1, \ldots, N, \tag{5.2}$$

where ℓ_{ij}^{SP} denotes the length of the shortest admissible path between vertices i and j (we consider only paths whose length is below the fixed threshold R_{C}), and $\tilde{\delta}_{\text{K}} = 1$. This formulation does not account for the multiplicity of connections, and therefore lacks the cumulative nature that characterizes the current approach. Tables 5 and 6 report the obtained results: none of these approaches successfully reproduced the deterioration pattern observed in the clinical data, neither in the case of the six ROIs nor in the case of the ten ROIs, thus further supporting the relevance of incorporating cumulative connectivity into the model.

Remark 1. Based on numerous numerical experiments, we observed that fairly wide intervals of parameter values exist, within which the obtained results are consistently reproduced, whereas outside these ranges, the outcomes can significantly vary. In this sense, the model exhibits a degree of robustness, as selecting parameter values within these intervals ensures reproducible results. While a more systematic sensitivity analysis could provide further insights, the current study focused on demonstrating the feasibility of the proposed approach rather than exhaustively exploring the parameter space.

Remark 2. For the sake of simplicity, we presented the parameters listed in Table 2 as fixed, while only allowing the parameters γ_3 and $C_{\mathbf{w}}$ to vary, as these appear in the equation that governs the evolution of the τ protein. However, it is important to emphasise that an exhaustive numerical exploration was performed in which all parameters were systematically varied. No alternative parameter values were found that produced better results than those obtained with the values reported in Table 2.

6. Discussion and conclusions

This study pursued two primary goals: first, to compare various modeling approaches for τ protein spread in the AD brain, thereby specifically considering the synergistic presence of Aβ protein; and second, to assess the model's validation by comparing generated numerical data with clinical data. Indeed, we firmly believe that a comparison between the theoretical model results and clinical data is necessary to establish the practical utility of mathematical models in AD research. To achieve this, we developed models where both proteins evolved on specialized networks derived from human connectomes and we introduced a new concept of deterioration pattern, which enabled us to make the comparison mentioned above. The distinct physiological and biological characteristics of Aβ and τ proteins necessitated different connectome structures. For Aβ, which propagates over short distances, we utilized a novel intrinsic proximity connectome with a standard diffusion Laplacian. For the τ protein, which is hypothesized to spread prion-like over longer distances, we investigated distinct mathematical models across different networks: diffusion via Laplacian on a newly introduced cumulative connectome, and spreading through a convolution operator on two structural connectomes. An important novelty of this paper concerns the definition of a new convolution kernel, which takes the cumulative nature of the connections between brain regions into account and appears to provide the best performance in terms of a comparison with clinical data. Indeed the numerical results obtained show that each operator K was able to reproduce only one of the two clinical deterioration patterns, but not both, even when the model parameters were varied.

In particular, the diffusion operator on the cumulative connectome $\mathcal{G}_{\mathrm{c}}$ successfully reproduced the pattern TLOS, but failed to match TFOLS. Similarly, the convolution operator on the structural graph $\mathcal{G}_{\mathrm{NL}}$ also only reproduced TLOS. On the other hand, the convolution operator on the length-based graph $\mathcal{G}_{\mathrm{L}}$ was the only one capable of reproducing TFOLS. The fact that no operator could reproduce both patterns, even with different parameter settings, suggests that the mathematical structure of the model, including the underlying graph, must be carefully tailored to the specific phenomenon under investigation.

It is worth noting that in our previous work, we also considered a convolution operator on the graph $\mathcal{G}_{\mathrm{NL}}$, but with a different kernel. In that case, the model was not able to reproduce the TLOS pattern, thus further confirming that the choice of both the graph and the convolution kernel plays a crucial role in shaping the modeled dynamics.

The proposed approach presents several limitations. First, the availability of medical data was restricted, which constrained the robustness of the analysis. Furthermore, the connectome employed in this study was derived from healthy brains, thus potentially limiting its applicability to pathological conditions. Additionally, the fitting of the τ protein concentration was not performed on longitudinal data, thus reducing the ability to capture the temporal dynamics. Finally, the comparative modeling framework was not applied to the dynamics of the $A\beta$ protein, which represents another important pathological marker. As future work, we plan to construct a connectome based on diseased brains and expand the medical dataset to enhance the reliability of the model. Moreover, we aim to apply the same comparative approach used for τ to validate the model's predictions for $A\beta$ dynamics. This will allow us to further assess the model's ability to reproduce observed patterns of pathology and its consistency with medical observations.

Use of AI tools declaration

The authors declare they have not used Artificial Intelligence (AI) tools in the creation of this article.

Institutional review board statement

As per ADNI protocols, all procedures performed in studies involving human participants were in accordance with the ethical standards of the institutional and/or national research committee and with the 1964 Helsinki declaration and its later amendments or comparable ethical standards. More details can be found at adni.loni.usc.edu. (This article does not contain any studies with human participants performed by any of the authors)

Informed consent statement

Authors received the consent of publication from ADNI.

Data availability statement

Data used in preparation of this article were obtained from the Alzheimer's Disease Neuroimaging Initiative (ADNI) database (adni.loni.usc.edu). As such, the investigators within the ADNI contributed to the design and implementation of ADNI and/or provided data but did not participate in analysis or writing of this report. A complete listing of ADNI investigators can be found at: http://adni.loni.usc.edu/wp-content/uploads/how_to_apply/ADNI_Acknowledgement_List.pdf. The publicly available datasets analyzed in this study can be found at these urls: http://adni.loni.usc.edu and https://braingraph.org, see [23, 32].

All data produced by the authors are available upon request from the authors.

Acknowledgments

G. L. is member of the Gruppo Nazionale per il Calcolo Scientifico (GNCS) of the Istituto Nazionale di Alta Matematica (INdAM) and this work was partially supported by INdAM-GNCS under Progetti

di Ricerca 2024 and 2025. A. S. and M. C. T. are members of the Gruppo Nazionale per l' Analisi Matematica, la Probabilita' e le loro Applicazioni (GNAMPA) of INdAM, Italy.

Data collection and sharing for this project was funded by the Alzheimer's Disease Neuroimaging Initiative (ADNI) (National Institutes of Health Grant U01 AG024904) and DOD ADNI (Department of Defense award number W81XWH-12-2-0012). ADNI is fundedby the National Institute on Aging, the National Institute of Biomedical Imaging and Bioengineering, and through generous contributions from the following: AbbVie, Alzheimer's Association; Alzheimer's Drug Discovery Foundation; Araclon Biotech; BioClinica, Inc.; Biogen; Bristol-Myers Squibb Company; CereSpir, Inc.; Cogstate; Eisai Inc.; Elan Pharmaceuticals, Inc.; Eli Lilly and Company; EuroImmun; F. Hoffmann-La Roche Ltd and its affiliated company Genentech, Inc.; Fujirebio; GE Healthcare; IXICO Ltd.; Janssen Alzheimer Immunotherapy Research & Development, LLC.; Johnson & Johnson Pharmaceutical Research & Development LLC.; Lumosity; Lundbeck; Merck & Co., Inc.; Meso Scale Diagnostics, LLC.; NeuroRx Research; Neurotrack Technologies; Novartis Pharmaceuticals Corporation; Pfizer Inc.; Piramal Imaging; Servier; Takeda Pharmaceutical Company; and Transition Therapeutics. The Canadian Institutes of Health Research is providing funds to support ADNI clinical sites in Canada. Private sector contributions are facilitated by the Foundation for the National Institutes of Health (www.fnih.org). The grantee organization is the Northern California Institute for Research and Education, and the study is coordinated by the Alzheimer's Therapeutic Research Institute at the University of Southern California. ADNI data are disseminated by the Laboratory for Neuro Imaging at the University of Southern California.

Conflict of interest

The authors declare there is no conflict of interest.

References

1. *Alzheimer's Disease International*, *Alzheimer's Disease Report*. Available from: https://www.alzint.org.
2. L. M. Ittner, J. Götz, Amyloid-β and tau—A toxic pas de deux in Alzheimer's disease, *Nat. Rev. Neurosci.*, **12** (2011), 67–72. https://doi.org/10.1038/nrn2967
3. G. S. Bloom, Amyloid-β and tau: The trigger and bullet in Alzheimer disease pathogenesis, *JAMA Neurol.*, **71** (2014), 505–508. https://doi.org/10.1001/jamaneurol.2013.5847
4. O. G. Tatarnikova, M. A. Orlov, N. V. Bobkova, Beta-amyloid and tau-protein: Structure, interaction, and prion-like properties, *Biochemistry (Mosc.)*, **80** (2015), 1800–1819. https://doi.org/10.1134/S000629791513012X
5. R. E. Bennett, S. L. DeVos, S. Dujardin, B. Corjuc, R. Gor, J. Gonzalez, et al., Enhanced tau aggregation in the presence of Amyloid β, *Am. J. Pathol.*, **187** (2017), 1601–1612. https://doi.org/10.1016/j.ajpath.2017.03.011
6. S. A. Small, K. Duff, Linking Aβ and Tau in late-onset Alzheimer's disease: A dual pathway hypothesis, *Neuron*, **60** (2008), 534–542. https://doi.org/10.1016/j.neuron.2008.11.007
7. R. Ossenkoppele, G. D. Rabinovici, R. Smith, H. Cho, M. Schöll, O. Strandberg, et al., Discriminative accuracy of [18F] flortaucipir positron emission tomography for Alzheimer disease vs other neurodegenerative disorders, *JAMA*, **320** (2018), 1151–1162. https://doi.org/10.1001/jama.2018.12917

8. Z. Ahmed, J. Cooper, T. K. Murray, K. Garn, E. McNaughton, H. Clarke, et al., A novel *in vivo* model of tau propagation with rapid and progressive neurofibrillary tangle pathology: The pattern of spread is determined by connectivity, not proximity, *Acta Neuropathol.*, **127** (2014), 667–683. https://doi.org/10.1007/s00401-014-1254-6
9. H. Braak, E. Braak, Neuropathological stageing of Alzheimer-related changes, *Acta Neuropathol.*, **82** (1991), 239–259. https://doi.org/10.1007/BF00308809
10. M. J. Grothe, H. Barthel, J. Sepulcre, M. Dyrba, O. Sabri, S. J. Teipel, et al., *In vivo* staging of regional amyloid deposition, *Neurology*, **89** (2017), 2031–2038. https://doi.org/10.1212/WNL.0000000000004643
11. M. A. Busche, B. T. Hyman, Synergy between amyloid-β and tau in Alzheimer's disease, *Nat. Neurosci.*, **23** (2020), 1183–1193. https://doi.org/10.1038/s41593-020-0687-6
12. T. B. Thompson, P. Chaggar, E. Kuhl, A. Goriely, Protein–protein interactions in neurodegenerative diseases: A conspiracy theory, *PLoS Comput. Biol.*, **16** (2020), e1008267. https://doi.org/10.1371/journal.pcbi.1008267
13. M. Bertsch, B. Franchi, A. Raj, M. C. Tesi, Macroscopic modelling of Alzheimer's disease: Difficulties and challenges, *Brain Multiphys.*, **2** (2021), 100040. https://doi.org/10.1016/j.brain.2021.100040
14. J. A. McNab, B. L. Edlow, T. Witzel, S. Y. Huang, H. Bhat, K. Heberlein, et al., The Human Connectome Project and beyond: Initial applications of 300 mT/m gradients, *Neuroimage*, **80** (2013), 234–245. https://doi.org/10.1016/j.neuroimage.2013.05.074
15. M. Bertsch, B. Franchi, M. C. Tesi, V. Tora, The role of Aβ and Tau proteins in Alzheimer's disease: A mathematical model on graphs, *J. Math. Biol.*, **87** (2023), 49. https://doi.org/10.1007/s00285-023-01985-7
16. S. Fornari, A. Schäfer, M. Jucker, A. Goriely, E. Kuhl, Prion-like spreading of Alzheimer's disease within the brain's connectome, *J. R. Soc. Interface*, **16** (2019), 20190356. https://doi.org/10.1098/rsif.2019.0356
17. A. Raj, A. Kuceyeski, M. Weiner, A network diffusion model of disease progression in dementia, *Neuron*, **73** (2012), 1204–1215. https://doi.org/10.1016/j.neuron.2011.12.040
18. F. Carbonell, Y. Iturria-Medina, A. C. Evans, Mathematical modeling of protein misfolding mechanisms in neurological diseases: A historical overview, *Front. Neurol.*, **9** (2018), 37. https://doi.org/10.3389/fneur.2018.00037
19. S. Moravveji, N. Doyon, J. Mashreghi, S. Duchesne, A scoping review of mathematical models covering Alzheimer's disease progression, *Front. Neuroinform.*, **18** (2024), 1281656. https://doi.org/10.3389/fninf.2024.1281656
20. J. Torok, C. Anand, P. Verma, A. Raj, Connectome-based biophysics models of Alzheimer's disease diagnosis and prognosis, *Transl. Res.*, **254** (2023), 13–23. https://doi.org/10.1016/j.trsl.2022.08.008
21. J. W. Vogel, N. Corriveau-Lecavalier, N. Franzmeier, J. B. Pereira, J. A. Brown, A. Maass, et al., Connectome-based modelling of neurodegenerative diseases: Towards precision medicine and mechanistic insight, *Nat. Rev. Neurosci.*, **24** (2023), 620–639. https://doi.org/10.1038/s41583-023-00731-8

22. S. Bianchi, G. Landi, C. Marella, M. C. Tesi, C. Testa, A network-based study of the dynamics of Aβ and τ proteins in Alzheimer's disease, *Math. Comput. Appl.*, **29** (2024), 113. https://doi.org/10.3390/mca29060113
23. B. Szalkai, C. Kerepesi, B. Varga, V. Grolmusz, Parameterizable consensus connectomes from the Human Connectome Project: The Budapest Reference Connectome Server v3.0, *Cogn. Neurodyn.*, **11** (2017), 113–116. https://doi.org/10.1007/s11571-016-9407-z
24. M. Meyer-Luehmann, T. L. Spires-Jones, C. Prada, M. Garcia-Alloza, A. de Calignon, A. Rozkalne, et al., Rapid appearance and local toxicity of amyloid-β plaques in a mouse model of Alzheimer's disease, *Nature*, **451** (2008), 720–724. https://doi.org/10.1038/nature06616
25. S. Dujardin, B. T. Hyman, Tau prion-like propagation: State of the art and current challenges, *Adv. Exp. Med. Biol.*, **1184** (2020), 305–325. https://doi.org/10.1007/978-981-32-9358-8_23
26. M. Goedert, M. G. Spillantini, Propagation of Tau aggregates, *Mol. Brain*, **10** (2017), 18. https://doi.org/10.1186/s13041-017-0298-7
27. A. Grigor'yan, *Introduction to Analysis on Graphs*, American Mathematical Society, **71** (2018).
28. H. Braak, K. Del Tredici, Alzheimer's pathogenesis: Is there neuron-to-neuron propagation, *Acta Neuropathol.*, **121** (2011), 589–595. https://doi.org/10.1007/s00401-011-0825-z
29. B. Ricaud, P. Borgnat, N. Tremblay, P. Gonçalves, P. Vandergheynst, Fourier could be a data scientist: From graph Fourier transform to signal processing on graphs, *C. R. Phys.*, **20** (2019), 474–488. https://doi.org/10.1016/j.crhy.2019.08.003
30. D. I. Shuman, S. K. Narang, P. Frossard, A. Ortega, P. Vandergheynst, The emerging field of signal processing on graphs: Extending high-dimensional data analysis to networks and other irregular domains, *IEEE Signal Process. Mag.*, **30** (2013), 83–98. https://doi.org/10.1109/MSP.2012.2235192
31. J. R. Dormand, P. J. Prince, A family of embedded Runge–Kutta formulae, *J. Comput. Appl. Math.*, **6** (1980), 19–26. https://doi.org/10.1016/0771-050X(80)90013-3
32. B. Szalkai, C. Kerepesi, B. Varga, V. Grolmusz, High-resolution directed human connectomes and the consensus connectome dynamics, *PLoS One*, **14** (2019), e0215473. https://doi.org/10.1371/journal.pone.0215473

AIMS Press